ELSEVIER

0142-9612(95)00339-8

Biomaterials 17 (1996) 1803–1812

0142-9612/96/$15.00

Studies on radio-opaque polymeric biomaterials with potential applications to endovascular prostheses

Marc-Anton B. Kruft*†, Abderazak Benzina*, Ron Blezer* and Leo H. Koole*

*Maastricht Centre for Biomaterials Research (MCBR), University of Limburg, P.O. Box 616, 6200 MD, Maastricht; †Eindhoven Polymer Laboratories (EPL), Eindhoven University of Technology, Eindhoven, The Netherlands

A new polymeric biomaterial, which uniquely combines radio-opacity (X-ray visibility) and low thrombogenicity, is described. First, preparation, purification, and identification of the essential monomeric building block, 2-[2'-iodobenzoyl]-ethyl methacrylate (**3**), are outlined. Second,

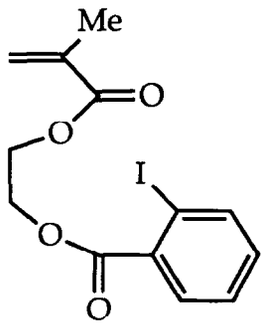

3

the synthesis of the biomaterial, a terpolymer with composition MMA : HEMA : 3 = 65 : 15 : 20 (mole/mole/mole) is described. Third, the physico-chemical characteristics of the polymer (e.g. NMR spectroscopy, thermal behaviour) are given. Fourth, the *in vitro* thrombogenicity of the material was characterized by means of recent test assay. The combined results reveal that the terpolymer is very suitable for prosthetic applications in the cardiovascular system. A new prototype of an endovascular stent, made from the terpolymer, is presented. Stents find clinical use in interventional cardiology, in conjunction with percutaneous transluminal coronary angioplasty (PTCA). It is put forward that the stent prototype presented herein has, at least in principle, some advantages over existing (metallic) stents; these advantages are primarily owing to the unique combination of X-ray visibility and haemocompatibility which is presently achieved. © 1996 Elsevier Science Limited.

Keywords: Radio-opacity, haemocompatibility, processability, stents, radio-opaque biomaterials

Received 23 June 1995; accepted 25 September 1995

Biomaterials are materials of synthetic or natural origin, used in contact with tissue, blood, or another biological fluid and intended for use in prosthetic, diagnostic, therapeutic, or storage applications[1–3]. Our research work is focussed in part on the chemical synthesis and further development of a new class of radio-opaque polymeric biomaterials i.e. biocompatible polymers with the capability of absorbing X-rays. In many clinical applications, it is highly desirable that an implant can be visualized via routine X-ray fluoroscopy. This allows the physician to monitor location and some aspects of the function of implants in a non-invasive manner. Evidently, this practice is straightforward for metallic implants. Polymeric materials, however, are normally transparent to X-radiation. In some applications, polymeric biomaterials are made radio-opaque via addition of a filler, usually an oxide or a salt of a relatively heavy element. For instance, bone cement—used in orthopaedic surgery for fixation of hip and knee prostheses to skeletal tissue—is made radio-opaque through addition of about 10 wt% of zirconium oxide (ZrO_2, Zr is element #40) or barium sulphate ($BaSO_4$, Ba is element #56)[4,5].

Correspondence to Dr Marc-Anton B. Kruft at MCBR.

An important drawback of this practice is that fillers do not mix with the polymeric (organic) matrix. This results in two highly undesirable effects[6,7]:

(i) the phase-boundaries between filler and polymer may become loci of initiation of mechanical failure (especially fatigue) in the course of time;
(ii) the filler may leach out of the material.

These considerations have inspired us to develop new polymeric biomaterials on the basis of radio-opaque monomeric building blocks[8,9]. Our approach was based on the synthesis of several methacrylate monomers, containing covalently bound iodine (e.g. **1,2**; iodine is element # 53).

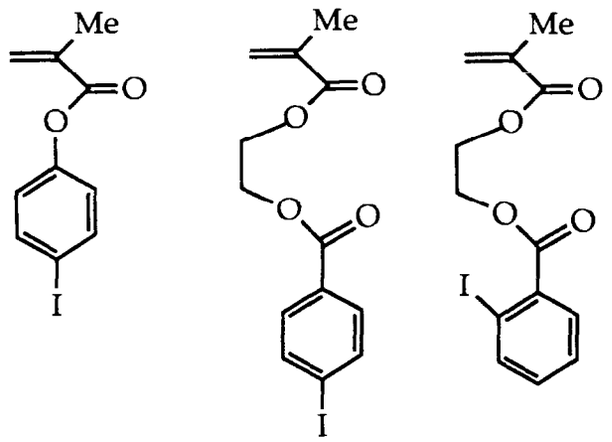

1 **2** **3**

Monomers **1** and **2** could readily be copolymerized with methyl methacrylate (MMA) and/or 2-hydroxyethyl methacrylate (HEMA).

Incorporation of HEMA, resulting in a more hydrophilic nature of the polymer, was found to improve the haemocompatibility, as reflected by an *in vitro* thrombin generation assay.

Herein, we report a comprehensive study on a new radio-opaque terpolymer, consisting of 2-[2′-iodobenzoyl]-ethyl methacrylate (**3**), MMA, and HEMA (mole ratio 20:65:15). Synthesis and physico-chemical characterization of this material is described. Furthermore, its *in vitro* haemocompatibility was tested with the thrombin generation assay as developed by Lindhout *et al.*[10], via an electron microscopic study of the morphology of adhered blood platelets, and by a dynamic flow test.

The material was used for the construction of a prototype of a new type of endovascular prosthesis (stent).

MATERIALS

Monomer preparation and purification

(i) MMA: Commercial MMA (200 mL, Janssen Chimica) was washed successively with sodium hydroxide (0.5 M, 100 mL, 3×), and water (100 mL, 3×), dried ($MgSO_4$), and filtered. The filtrate was distilled at atmospheric pressure (b.p. 101°C). A relatively large prerun (about 40 mL) was discarded. This procedure afforded pure MMA (>99.5%), as judged by 400 MHz ^{1}H-NMR spectroscopy. The product was stored at −20°C.

(ii) HEMA: Commercial HEMA (200 mL, Janssen Chimica) was distilled *in vacuo* (13 mbar, b.p. = 105°C) without pre-treatment. A relatively large prerun was discarded. ^{1}H-NMR (400 MHz) proved the purity of the distillate (>99.5%). The product was stored at −20°C.

(iii) Compound **3**: A solution of 2-iodobenzoyl chloride (10.00 g, 37.5 mmol) in 50 mL of dry dichloromethane was added dropwise over 60 min to a magnetically stirred and cooled (−5°C) solution of distilled HEMA (5.85 g, 45.0 mmol) and dry triethylamine (7.59 g, 75.0 mmol) in 150 mL of dry dichloromethane. After completion of the addition, the cooling bath was removed and stirring was continued for 1 h. Then, the yellow reaction mixture was again cooled to −5°C, and 200 mL of distilled water was added carefully. The reaction mixture was transferred to a separation funnel, the organic phase separated, and subsequently washed with saturated $NaHCO_3$ (150 mL, 1×) and brine (150 mL, 1×).

The organic layer was dried ($MgSO_4$), filtered and concentrated. The residue was chromatographed in two runs on a silica gel column (∅ 3 cm, height 20 cm) using petroleum ether 40–65 and ethyl acetate (90:10 v/v) as the eluent. Fractions containing pure product ($R_f = 0.39$ in the same eluent) were pooled and concentrated. This afforded the desired product as a viscous slightly yellowish oil. The yield was 10.81 g (80%). The product was stored at −20°C.

The purity and identity of compound **3** was verified by various analytical techniques, such as ^{1}H- and ^{13}C-NMR spectroscopy (see also Results).

^{1}H-NMR ($CDCl_3$): δ 7.99 (1H, d, arom), 7.79 (1H, d, arom), 7.41 (1H, t, arom), 7.16 (1H, t, arom), 6.17 (1H, s, olef. H *trans* to Me), 5.61 (1H, s, olef. H *cis* to Me), 4.60 and 4.56 (4H, 2 × m, OCH_2CH_2O) 1.98 (3H, s, Me).

^{13}C-NMR ($CDCl_3$): δ 167.07, 166.13, 141.34, 135.80, 134.60, 132.79, 131.06, 127.90, 126.26, 94.08, 63.17, 62.21, 18.30.

IR (KBr): 1731 (C=O), 1720 (C=O), 1640 (C=C, alkene), 1583 and 1457 cm^{-1} (C=C, aromatic).

Elemental analysis (calculated): C, 43.36; H, 3.64; I, 35.24. Found: C, 43.54; H, 3.66; I, 37.02.

Polymer preparation

Synthesis of the target polymer was carried out in a Teflon tube (length: 25 cm, inner diameter: 12 mm, outer diameter: 14 mm). The tube was tightly closed with a glass stopper on one end. For the synthesis in the Teflon tube, we used MMA (6.23 g, 62.3 mmol), HEMA (1.87 g, 14.4 mmol), and compound **3** (6.90 g, 19.2 mmol). Stock solutions were made of (i) radical initiator Trigonox-C: MMA = 1:19 (v/v), (ii) chain-transfer agent 2-mercaptoethanol : MMA = 1:19 (v/v).

Aliquots of these stock solutions were transferred into the Teflon tube, using a micropipette (see *Table 1*). The contents of the tube were thoroughly mixed and the tube was placed in a thermostated oil bath, equipped with a programmable time–temperature

control system (PM LAUDA, Königshofen, Germany). The time–temperature profile as depicted in *Figure 1* was then run.

This procedure afforded the material as a hard, transparent, colourless rod. The Teflon was removed using a scalping knife and the upper and lower part (1 cm each) of rods were cut off and discarded. Part of the remaining material was used for physical characterization. Three different syntheses were executed (*Table 1*). The first synthesis afforded polymer A (weight-average molecular weight: $M_w = 41.4\,kg\,mol^{-1}$); the second synthesis afforded polymer B ($M_w = 210\,kg\,mol^{-1}$), and the third synthesis afforded polymer C ($M_w = 182.0\,kg\,mol^{-1}$). Note that the polymers A–C have the same chemical composition: they merely differ with respect to M_w, M_n, and polydispersity.

^{1}H-NMR of polymer A: (DMSO-d_6): δ 8.13-7.94 (br, arom H), 7.86–7.68 (br, arom H), 7.61–7.41 (br, arom H), 7.39–7.18 (br, arom H), 4.88–4.67 (br, OH), 4.62–4.35 (br, CH_2 of iodine-containing monomer), 4.35–4.10 (CH_2 of iodine-containing monomer), 4.04–3.75 (br, CH_2 of HEMA), 3.65–3.40 (br, OMe and other CH_2 of HEMA), 3.34 (trace of H_2O), 2.50 (DMSO-d_6), 2.1–1.3 (br, CH_2 in chains), 1.2–0.5 (br, Me).

METHODS

Physico-chemical analysis

(i) Elemental analysis. Elemental analyses were performed by Galbraith Laboratories (Knoxville, TN, USA).

(ii) Nuclear magnetic resonance (NMR) in solution. ^{1}H- and ^{13}C-NMR spectra were recorded on a Varian Unity-Plus system (Varian, Palo Alto, USA) at 399.9 and 100.6 MHz, respectively. Chloroform-d was used as the solvent for the monomer and DMSO-d_6 was used as the solvent for the polymer. Tetramethylsilane was used as the internal standard ($\delta = 0.00$ ppm).

(iii) Solid-state NMR. The solid-state ^{13}C-NMR measurements were carried out on a Bruker MSL 400 Fourier Transform NMR spectrometer (Bruker Analytische Messtechnik, Rheinstetten, Germany) at 100.6 MHz. A sample of about 250 mg was measured in 4 mm O.D. rotors made of ZrO_2 of the Bruker double-bearing type. The proton 90° pulse length was 6.6 μs and the repetition time 1 s. The MAS spinning rates were 5.5 and 7.0 kHz. 4800 free induction decays (FIDs) with an acquisition time of 20 ms were accumulated in 1 k data points. During acquisition, ^{1}H decoupling was carried out.

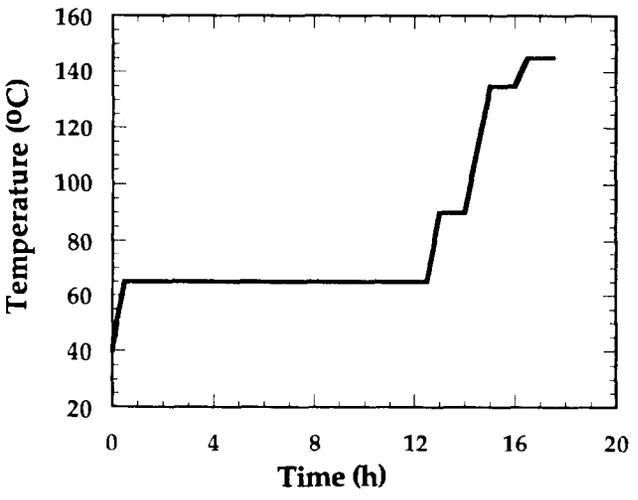

Figure 1 Time–temperature profile as used in the synthesis of polymers A–C. Cooling at the end of the synthesis was unforced; it took approximately 4 h before room temperature was reached.

Table 1 Concentrations of initiator and chain-transfer agent used during preparation of polymers A–C

Polymer	Initiator[a]		Chain-transfer agent[b]	
	μL of stock	Final conc.[c]	μL of stock	Final conc.[d]
A	244	0.068 mol%	1312	1.00 mol%
B	143	0.040 mol%	525	0.40 mol
C	143	0.040 mol%	–	–

[a]Initiator = *tert.*-butyl peroxybenzoate (Trigonox C®, Akzo, Deventer, The Netherlands); [b]chain-transfer agent = 2-mercaptoethanol (Janssen Chimica, Beerse, Belgium); [c]final concentration expressed as follows: (mmol initiator/(mmol MMA + mmol HEMA + mmol monomer 3)) × 100%; [d]final concentration expressed as follows: (mmol chain-transfer agent/(mmol MMA + mmol HEMA + mmol monomer 3)) × 100%.

(iv) Gel permeation chromatography (GPC). GPC was used to determine the M_w, the number-average molecular weight (M_n) and the polydispersity (M_w/M_n) of the polymer. GPC was performed using a Waters Wisp autoinjection apparatus (Millipore Corp., Milford, MA, USA), equipped with 10^5, 10^4, 10^3 μ-Styragel (Alltech, Deerfield, IL., USA) columns (Shodex KF 80 M 2×, 40°C). THF was used as the mobile phase at a flow rate of 1.0 mL min^{-1}. The GPC measurements were determined independently by UV (UV 440, ambient conditions) at 254 nm and refractive index (RI 410, 40°C). Calibration was performed with polystyrene standards ($580 - 6 \times 10^6\,g\,mol^{-1}$).

(v) Differential scanning calorimetry (DSC). The glass transition temperature (T_g) and the corresponding change of heat capacity (ΔC_p) were measured using a heating rate of 10°C min^{-1} and determined from the second heating scan using a Perkin Elmer DSC 7 (Perkin Elmer Inc., USA). T_g was taken as the midpoint of the transition region. Argon was used as the carrier gas. The DSC was calibrated using indium and zinc.

(vi) Thermogravimetric analysis (TGA). The degradation behaviour was investigated using a Perkin Elmer TGA-7 (Perkin Elmer Inc., USA) thermogravimetric analyser. Measurements were performed in air with a heating rate of 10°C min^{-1}.

(vii) Dynamic mechanical thermal analysis (DMTA). The polymer was compression moulded at 180°C into rectangular plates using a Fontijne press (Fontijne, Vlaardingen, The Netherlands). These plates were used for our dynamic mechanical thermal measurements. Dynamic mechanical thermal measurements were performed with a Polymer Laboratories Dynamic Mechanical Analyser (Polymer Laboratories Ltd., Loughborough, UK), operated in the tensile

mode. Rectangular plates (20 × 6 × 2 mm) were run at a measuring frequency of 1 Hz, a static force of 0.1 N, and a heating rate of 2.0°C min^{-1}.

Biochemical analysis

(i) General: in all biochemical experiments we used human blood obtained by venipuncture. Donors had not taken aspirin or other platelet-active agents for at least 7 d before donation. The blood was anti-coagulated through addition of a 130 mM trisodium-citrate solution (volume blood:volume citrate = 9:1).

Citrated whole blood from several donors was pooled in the preparation of platelet-free plasma (PFP). Centrifugation (twice at room temperature (15 min, 3000 g) and once at 4°C (60 min, 23 000 g)) afforded PFP, which was stored at −80°C.

Contact activation of plasma was performed by incubation of 470 μL of PFP with 3.5 μL of Tris buffer and 10 μL phospholipid (1 mM; 20 mol% phosphaditylserine/80 mol% phosphatidylchloline), followed by the addition of 20 μL $CaCl_2$ (0.5 M).

Platelet-rich plasma (PRP) was prepared from citrated whole blood by centrifugation at 1000 rpm for 10 min. Blood of a healthy human donor was used.

(ii) Static thrombogenicity tests: the static tests were performed with polymer films, obtained by film casting. Circular glass coverslips (∅ 20 mm), thoroughly cleaned with pure ethanol, were used. Film casting was done with a 10% (wt/wt) solution of the polymer in distilled dimethylformamide. The coated coverslips were pre-dried under clean room conditions and subsequently dried *in vacuo* just below the glass transition temperature of the polymer. Scanning electron microscopy indicated that the films were smooth, homogeneous, and particle-free. Glass coverslips coated with the polymer were placed in a 24-well titre plate and exposed to citrated PFP or PRP (500 μL) over 15 min at 37°C. The plate was shaken at 150 rpm on an orbit shaker (Lab-line Instruments, Metrose Park, USA). The surface to volume ratio (7.6 cm^2 mL^{-1}) was kept constant for all testings. Clotting was started through addition of Ca^{2+} ions (final free $[Ca^{2+}] = 4$ mM). In the PFP experiment the final concentration of phospholipid was 20 mM. Subsamples were taken and analysed for thrombin using the chromogenic substrate S2238 (H-D-Phe-Pip-Arg-pNA, KABI, Stockholm, Sweden) as previously described by Lindhout *et al.*[10].

(iii) Dynamic thrombogenicity tests: for the dynamic flow test we machined the polymeric material in rectangular plates (50 × 10 × 0.5 mm). This machining was done in such a way that smooth and clean surfaces were obtained.

A flat parallel plate perfusion chamber was used to study platelet adhesion under PRP flow conditions. The device used was a modification of the perfusion chamber described by Sakariassen *et al.*[11]. In a poly(methyl methacrylate) block (dimensions 75 × 26 × 7 mm), a central hole with a depth of 0.2 mm, a width of 5.0 mm, and a length of 28 mm was made. The chamber volume is 28 μL. The two inlets of the chamber (1 mm i.d.) gradually taper off over 7 mm to the rectangular cross-section of the central hole at an angle of 20°. A rectangular piece of the test material (dimensions: 50 × 10 × 0.5 mm) served as the roof of the flow chamber; approximately 1.5 cm^2 of the test surface was in contact with flowing PRP. The wall shear rate was calculated from the formula: shear rate = $6Q/bd^2$, where Q is the volumetric flow rate (cm^3 s^{-1}), b (cm), and d (cm) are width and depth of the slit, respectively. The flow was controlled by an infusion syringe pump (Harvard Apparatus Co, MA, USA).

The amount of adhered platelets under flow conditions was quantified by the determination of one of the enzymes of the platelets, lactate dehydrogenase (LDH). Before use, the rectangular plates were rinsed overnight with phosphate-buffered saline (PBS). The surface of the plates, used in the experiments, were flushed for 10 min with PBS and then flushed for 10 min with PRP. The non-adherent platelets were removed by flushing the polymer surface for 10 min with PBS. The shear rates used in all steps were 30, respectively 300 s^{-1}. The adherent platelets were lysed by exposing the surface for 5 min to 1% Triton X-100 in PBS. For determination of LDH content the sample was mixed with 0.5 mg ml^{-1} pyruvate and 240 μM of reduced nicotinamide adenine dinucleotide (NADH). LDH catalyses the conversion of pyruvate to lactate according to:

$$\text{Pyruvate} + \text{NADH} + \text{H}^+ \xrightarrow{\text{LDH}} \text{Lactate} + \text{NAD}^+$$

The disappearance of NADH was measured at 340 nm. A reference plot was constructed using known amounts of platelets.

(iv) Morphology of adhered platelets: glass coverslips, coated with polymer and incubated with citrated platelet-rich plasma for 30 min at 37°C, were rinsed with a saline buffer and treated with 2.5% glutaraldehyde in 0.1 M phosphate buffer at 4°C overnight. The samples were removed, rinsed with 0.1 M phosphate buffer and dehydrated in ethanol series (subsequently increasing from 50 to 100% ethanol). Identically, the plates used in the dynamic flow test were rinsed with saline buffer, treated with glutaraldehyde, rinsed with phosphate buffer, and dehydrated in ethanol series. Subsequently, the samples were dried by the critical point drying method. The dried samples were gold sputtered and subjected to scanning electron microscopic observations at an accelerating voltage of 15 kV using a Philips 505 SEM microscope (Philips, Eindhoven, The Netherlands).

RESULTS AND DISCUSSION

Physico-chemical analysis

Figure 2 shows the two-dimensional ^{13}C–^{1}H heterocorrelated NMR spectrum of compound **3**, dissolved in $CDCl_3$. The spectrum, along with the other analytical data (*vide supra*), clearly established the identity and purity of the monomeric building block.

Polymer A was also studied by 400 MHz ^{1}H-NMR; a small amount (about 10 mg) was dissolved in 0.5 mL of DMSO-d_6. Parts of the one-dimensional ^{1}H-NMR spectrum of polymer A are shown in *Figure 3*. The

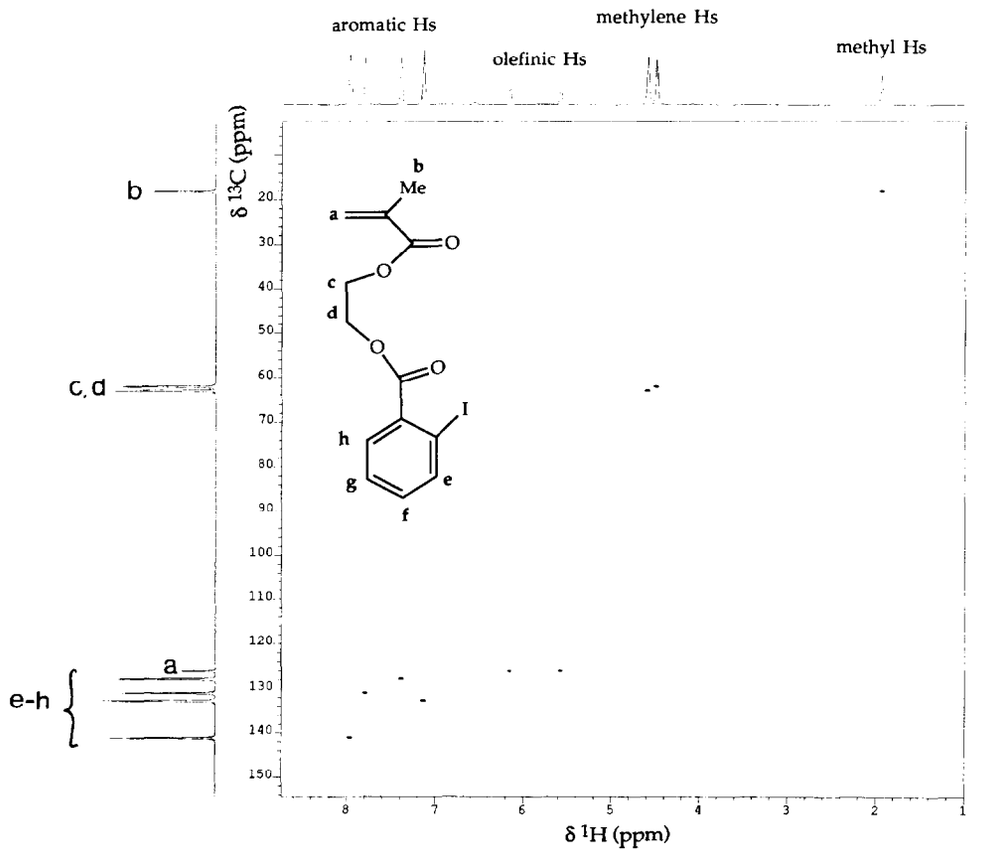

Figure 2 Two-dimensional ^{13}C–^{1}H heterocorrelated NMR-spectrum of compound **3**, dissolved in $CDCl_3$. The spectrum confirms the identity and purity of the iodine-containing monomer. Assignments of the ^{13}C resonances are given. Note that only C-atoms which are directly linked to one or more protons appear in the spectrum. Chemical shifts of all ^{13}C resonances (i.e. including those five that do not bear hydrogen) are given in the experimental section.

spectrum reveals the presence of the different constituents in the polymer. This is especially the case for the aromatic protons of the 2-iodophenoxy group which appear as broadened signals centred at 8.04, 7.77, 7.51 and 7.28 ppm (subspectrum c). Integration of these signals, and comparison with the integral of the Me groups attached to the polymer chain (1.2–0.5 ppm, subspectrum a), confirms the composition of the polymer. The NMR spectrum also shows the presence of traces of residual monomer. The small and sharp signals in subspectra a, b, and c are due to unreacted monomer molecules. Based on the NMR spectra, it is clear that the content of residual monomer in the polymer is below 1%.

Figure 4 shows the solid-state ^{13}C-NMR spectrum of polymer A at a MAS spinning rate of 5.5 kHz. The spinning side-bands (marked with an asterisk) were determined using MAS spinning rates of 5.5 and 7.0 kHz. The spectrum consists of nine signals, and clearly reveals the identity of the polymer. Note the signal near 95 ppm, which originates from the aromatic carbon, covalently attached to iodine. The intensity of this characteristic signal is relatively low, as only 20 mol% of monomer **3** was incorporated in the material.

Gel permeation chromatography was used to measure M_n and M_w. Two independent detection techniques, UV extinction and refractive index, were applied. Both techniques produced consistent results as summarized in *Table 2*.

These data revealed that we have obtained genuine polymeric materials. It can be concluded from *Table 2* that the M_w of the material can be influenced by changing the amount of peroxide and chain-transfer agent used during synthesis of the material. Thus, the iodine-containing monomer readily reacts with MMA and HEMA. At this point it is important to recall that Jayakrishnan *et al.*[12] found that triiodophenyl methacrylate and the iothalamic ester of HEMA are markedly resistant to copolymerization with MMA and/or HEMA. These authors assumed that steric hindrance owing to the iodine-containing aromatic moiety hampers efficient polymerization.

The results of the DSC experiments are compiled in *Table 3*.

A T_g value of 75°C was found for polymer A. For polymer B, a T_g value of 77°C was found. These T_g values are, as can be expected, almost equal. We also synthesized the homopolymer of compound **3**, and measured the T_g. A T_g value of 58°C was found. Using this value and applying the well-known Fox equation[13] for approximating the T_g of the material (using T_g (PMMA) = 105°C and T_g (PHEMA) = 55°C[14], a T_g value of 75°C for the material is calculated. Thus, the experimental and the calculated theoretical value of the T_g are in agreement.

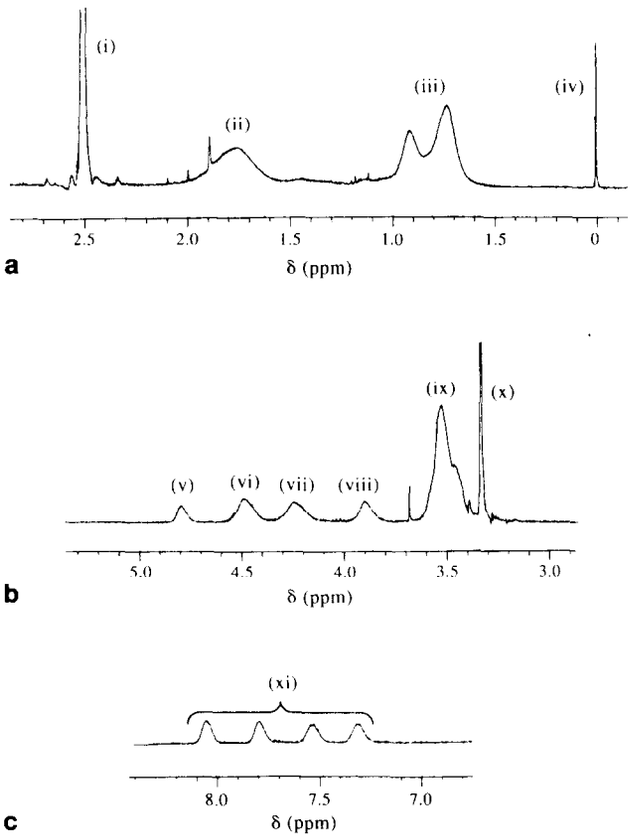

Figure 3 Expansions of the 400 MHz ^{1}H-NMR spectrum of polymer A dissolved in DMSO-d_6. Assignments are as follows (i): residual solvent signal: (ii): CH_2 groups in the polymer chains; (iii): Me groups, attached to the polymer chains; (iv): TMS; (v) OH groups of HEMA building blocks. It was verified that this peak disappears upon addition of a small amount of D_2O to the NMR sample; (vi) and (vii): side-chain CH_2 groups of the iodine-containing building blocks; (viii): one of the side-chain CH_2 groups of HEMA building blocks; (ix): MeO groups and the other side-chain CH_2 group of HEMA building blocks; (x): trace of H_2O; (xi): aromatic protons; note that these signals arise from the inequivalent positions on the aromatic ring. Signal integrations confirmed the polymer composition. mmol MMA:mmol HEMA:mmol **3** = 65:15:20 (see text).

Figure 5 shows the weight loss of a sample of polymer A at a heating rate of 10°C min^{-1}. Degradation of polymer A starts at about 300°C, which proves the stability of the material. In particular, these data reveal thermal stability of the C–I bond. Thermal degradation of polymer A and PMMA appear to be highly comparable (unpublished results).

Figure 6 shows log E^* versus temperature as measured in the tensile mode for polymer B. E^* refers to the dynamic modulus[15].

The most important information that can be obtained from *Figure 6* is: (i) the point of inflection at about 101°C, which corresponds to the transition from glassy state to rubbery state. (The difference between T_g (77°C) and the point of inflection as measured by DMTA (101°C) can be explained by the fact that DSC and DMTA are static and dynamic methods, respectively and by the fact that different heating rates were used.) The transition from glassy to rubbery state was confirmed by the corresponding internal friction (tan δ) curve as a function of temperature. It was seen that this curve passes a maximum at 101°C; (ii) the curve shows a rubber plateau in the range 140–180°C. The presence of the rubber plateau reveals substantial entanglement of the polymer chains. Furthermore, the occurrence of a rubbery plateau points out that the mechanical properties of polymer B are close to ultimate; (iii) the curve also shows that polymer B flows viscously in the range 180–205°C. This is due to disentanglement of the polymer chains.

As is well known, the mechanical properties of polymers improve as the molecular weight increases. However, beyond some critical molecular weight, usually about 100–200 kg mol^{-1} for amorphous polymers, the increase in property values is slight and levels off asymptotically[16].

Note that the presence of a rubber plateau in *Figure 6* correlates well with the GPC results, which showed $M_w = 210$ kg mol^{-1} for polymer B.

In our opinion, the combined results of the thermal analyses of polymer B show that this material is processable, e.g. the material can be used in injection moulding. In other words, it must be anticipated that objects with complex shapes can be manufactured from polymer B and related radio-opaque materials.

In vitro thrombogenicity

Polymer A was subjected to the static *in vitro* thrombin generation test procedure as recently described by Lindhout *et al.*[10]. This test procedure can be executed with PFP or PRP, and provides a valuable impression of the thrombogenicity of foreign surfaces. The tests are essentially comparative, i.e. control experiments with reference surfaces must be executed simultaneously under the same experimental conditions and with the same plasma. The reference materials were polyethylene (PE) and polyvinyl chloride (PVC), which contains tri-(ethyl-hexyl)-trimellitat as plasticizer. Both reference materials were obtained from the EC program "Eurobiomat". Circular glass coverslips (∅ 20 mm) coated with polymer A were used. The PFP and PRP thrombin generation experiments were performed *in duplo* and *in triplo*, respectively. *Figure 7* shows the thrombin generation curve, measured for PRP exposed to polymer A.

In general, a thrombin generation curve shows a lag phase which is followed by a shorter phase in which formation of thrombin proceeds in an explosive manner. Subsequently, the thrombin concentration is seen to pass a maximum. We have used the thrombin generation curves merely to obtain two parameters, which are directly related to the thrombogenicity of the material. The first parameter is the duration of the lag phase (lag time), and the second parameter is the maximum concentration of free thrombin reached during the experiment.

Note that the lag time corresponds to the classical clotting time, as the increase of thrombin concentration will directly start the formation of fibrin. The results of our experiments with polymer A, and the reference materials PE and PVC, are presented in *Tables 4* and *5*. Furthermore, an uncoated glass coverslip was used as a third control surface. The

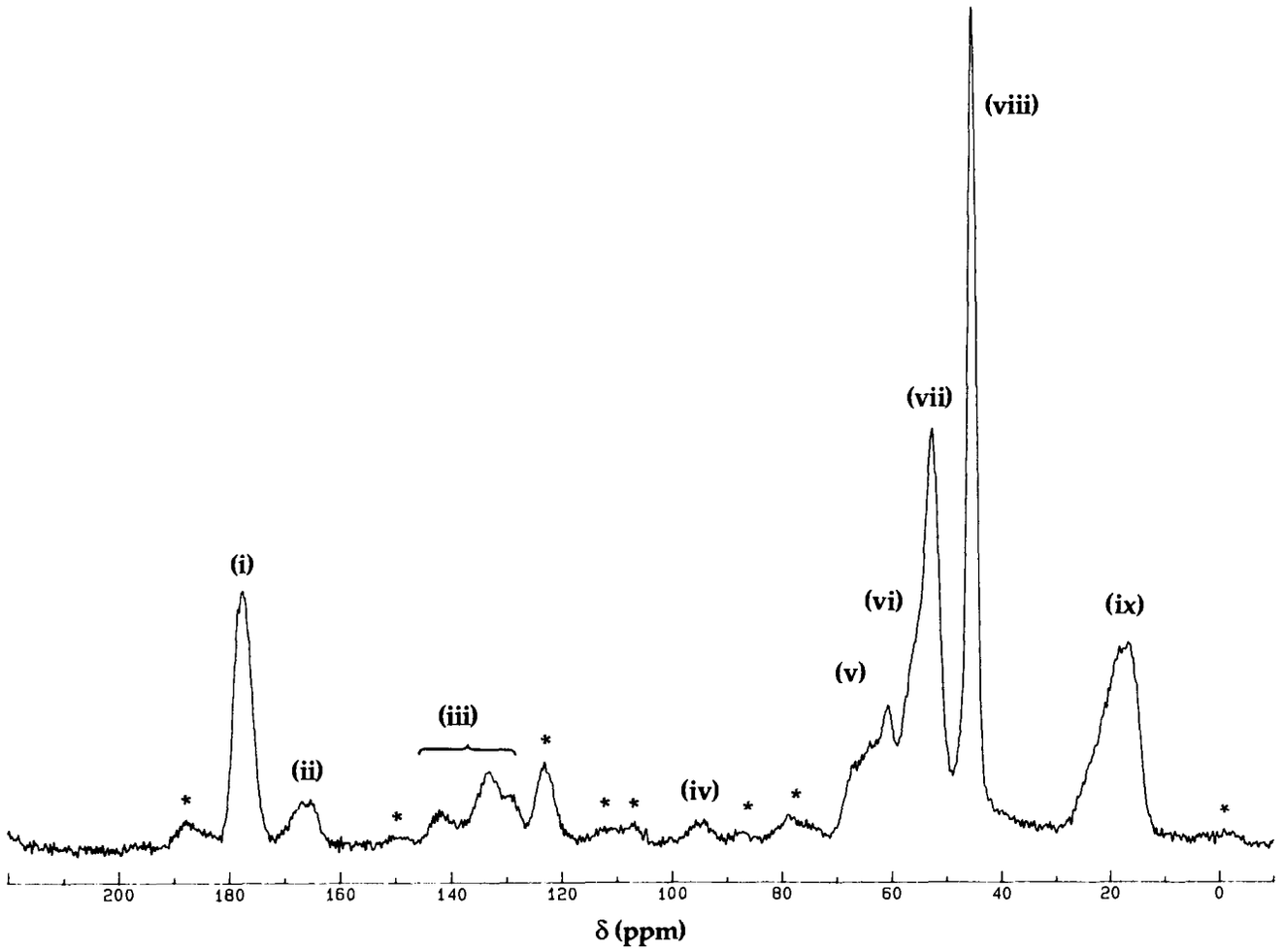

Figure 4 Solid-state ^{13}C-NMR spectrum of polymer A (cross-polarization, magic angle (5.5 kHz)). Spinning side-bands are indicated by asterisks. Signals and spinning side-bands were distinguished unequivocally via a comparison with the analogous spectrum, recorded at the spinning frequency of 7 kHz. Assignments are as follows: (i): C=O groups, attached to the polymer chains; (ii): C=O groups of 2-iodobenzoyl; (iii): aromatic carbons, except C-I; (iv): aromatic carbon, attached to iodine; (v) OCH_2 of HEMA building blocks and OCH_2 of **3** building blocks; (vi): CH_2 groups of the polymer chains; (vii): OMe groups; (viii): quaternary carbons in the polymer chains; (ix): Me groups, attached to the polymer chains.

maximum thrombin concentrations listed were obtained after correction of the experimental thrombin generation curve for the residual amidolytic activity of the thrombin–α_2 macroglobulin complex (thrombin–α_2M). The procedure of Hemker *et al.*[17] was applied to perform this correction. The polymeric reference materials were examined as foils, not as a coating on glass. (In the case of PVC, we showed[8] that the same lag time is found for the polymer as a film, and for the polymer as a coating on glass.)

Table 4 compiles the results of the experiments with PFP. As can be seen, both the lag time and the

Table 2 Results from gel permeation chromatography on polymers A–C. Data refer to refractive index as the detection technique

Polymer	M_n (kg mol^{-1})	M_w (kg mol^{-1})	M_w/M_n
A	16.5	41.4	2.51
B	72.5	210	2.89
C	52.0	182	3.50

Table 3 Glass transition temperature and change of heat capacity of polymers A and B

Polymer	T_g (°C)	ΔC_p (J/g°C)
A	75	0.2
B	77	0.2

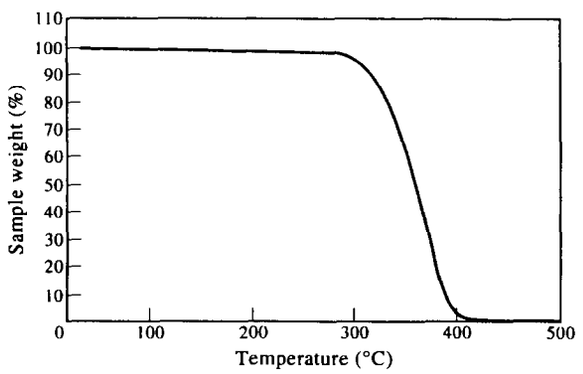

Figure 5 Thermal degradation of polymer A in air. The heating rate was 10°C min^{-1}.

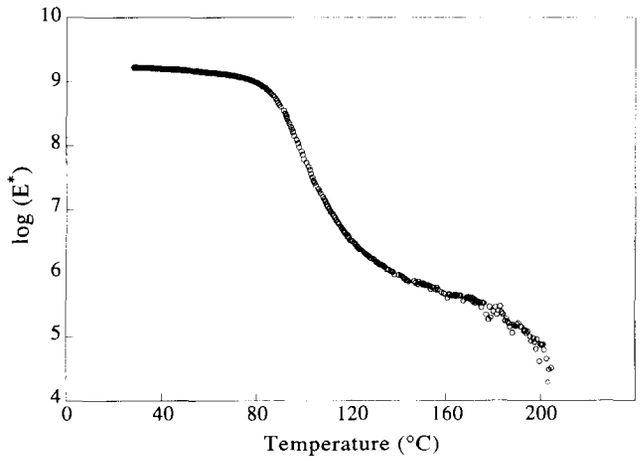

Figure 6 Results of the DMTA experiments on polymer B. The graph shows log E^* (E^* = dynamic modulus) as function of temperature.

maximal thrombin concentration of PE, PVC and polymer A are almost equal. It can be concluded that the contribution of contact activation to coagulation is the same for all these polymeric materials. For glass,

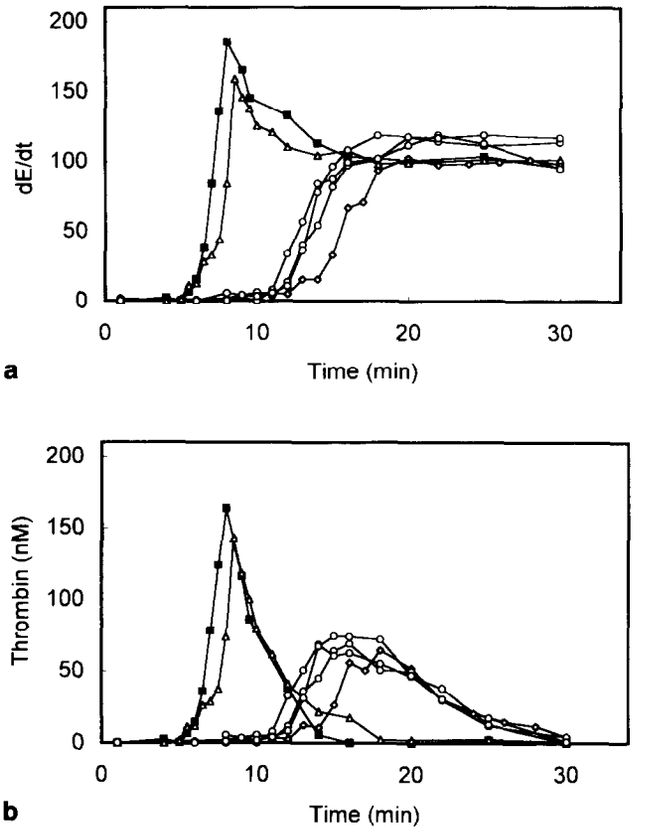

Figure 7 **a,** Experimental curve for the thrombin generation test executed with PRP, $d(E)/dt$ (arbitrary units; E = extinction) is shown as a function of time. The residual amidolytic activity at the end of the experiment (time > 15 min) is due to the thrombin-α_2 macroglobulin complex. **b,** Thrombin concentration as a function of time; a correction for the amidolytic activity of the thrombin–α_2 macroglobulin complex was performed according to the procedure of Hemker *et al.* (see Ref. 17). Codes for **a** and **b**: △ = glass, ■ = polyethylene, ○ = Polymer A (experiment in triplo), ◇ = PVC.

Table 4 Results of PFP thrombin generation tests for coated polymer A, glass, and reference materials

Material	Lag time (s)	Max. thromb. conc. (nM)*
Glass	224	194
PE	537	240
PVC	557	267
Polymer A[1]	638 ± 16	211 ± 15

[1]Experiments with coated polymer A were performed *in duplo*; the reported lag time and maximal thrombin concentrations are averages of two experiments; the standard deviations are also given.
*Calculated for thrombin generation curves according to Hemker *et al.*[17].

Table 5 Results of PRP thrombin generation tests for coated polymer A, glass, and reference materials

Material	Lag time (s)	Max. thromb. conc. (nM)*
Glass	288	150
PE	345	171
PVC	705	74
Polymer A[1]	599 ± 12	81 ± 6

[1]Experiments with coated polymer A were performed *in triplo*; the reported lag time and maximal thrombin concentrations are averages of three experiments; the standard deviations are also given.
*Calculated for thrombin generation curves according to Hemker *et al.*[17].

on the contrary, the contribution of contact activation to coagulation is clearly more significant.

Table 5 shows the results of the experiments with PRP. Polymer A is less thrombogenic than PE and glass, but somewhat more thrombogenic than PVC in terms of lag-phase duration. Comparing the maximal thrombin concentrations reached with the polymer and PVC, it is seen that [thrombin] of polymer A is only slightly higher than that of PVC. It should be noted that clotting times are slightly donor-dependent.

PE, which is very thrombogenic, has a typical clotting time of approximately 300 s. The more passive material PVC usually has a clotting time of approximately 700 s.

In another experiment, polymer A was incubated with citrated platelet-rich plasma for 30 min at 37°C. *Figure 8a* shows a representative scanning electron micrograph of the surface. Some adhered blood platelets are clearly visible. *Figure 8b* provides a detailed picture of the morphology of these platelets. Some extend small pseudopods, i.e. only a minor change in platelet morphology has occurred upon adsorption to the polymer. It is interesting to compare the results with the controls— platelets of the same plasma adhered to the reference materials PE and PVC. For PE, extensive spreading of the platelets was found, in such a way that most of the surface was covered. For glass, total covering of the surface with platelets was found. Only a few adhered platelets were found for PVC; in fact, these SEM micrographs resemble those found for polymer A. It can be concluded that polymer A and PVC behave in a highly similar way with respect to platelet activation. These findings correspond well with the results of the thrombin generation tests.

Table 6 shows the results of the dynamic thrombogenicity test for polymer C at two different

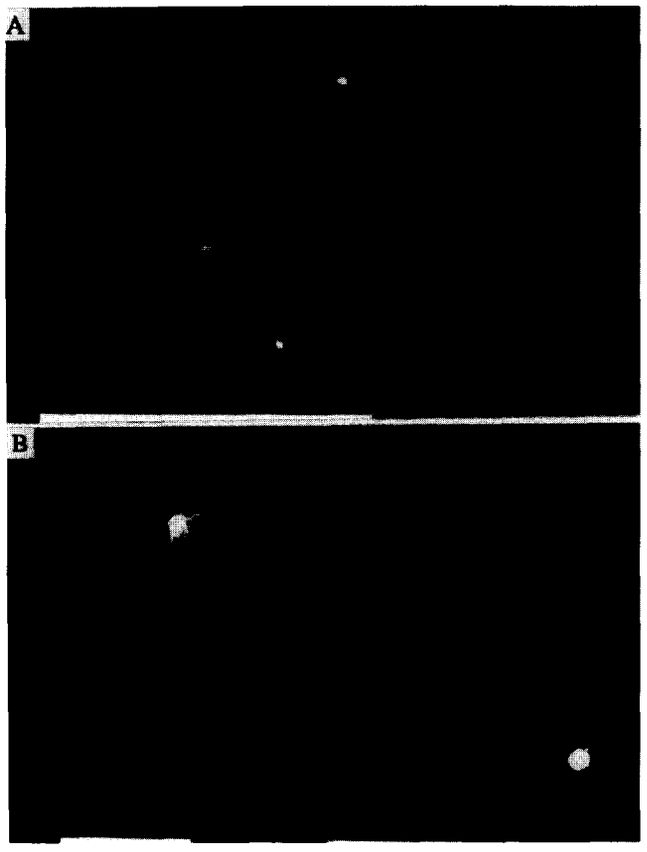

Figure 8 SEM images of polymer A after incubation with platelet-rich plasma for 30 min at 37°C. **A,** Typical overview. The length of the bar = 0.1 mm. **B,** Detail of the same specimen showing the morphology of adhered platelets. Formation of small pseudopods is noted. Scale bar = 10 μm.

shear rates: 30 and 300 s^{-1}. The data in *Table 6* reveal that the number of adhered platelets per cm^2 is comparable for polymer C and PVC, while the density of adhered platelets on PE is much higher. The same results are obtained from SEM experiments.

Stent prototype

The physico-chemical and biochemical analyses performed with polymers A–C suggest that these materials are particularly attractive for prosthetic applications in the cardiovascular circuit. In particular, polymers B and C appear very suitable for the construction of a new type of polymeric coronary stent[18]. A stent provides a 'scaffolding' which, in the ideal case, supports the damaged coronary vessel wall, prevents recoil of the vessel wall, and improves blood flow by smoothing the luminal surface. The use of stents is becoming increasingly important in interventional cardiology, as balloon angioplasty (PTCA) has

Table 6 Results of dynamic thrombogenicity test

Material	Platelets cm^{-2} Shear rate = 30 s^{-1}	Platelets cm^{-2} Shear rate = 300 s^{-1}
PE	521 000	345 000
PVC	111 000	35 000
Polymer C	130 000	63 000

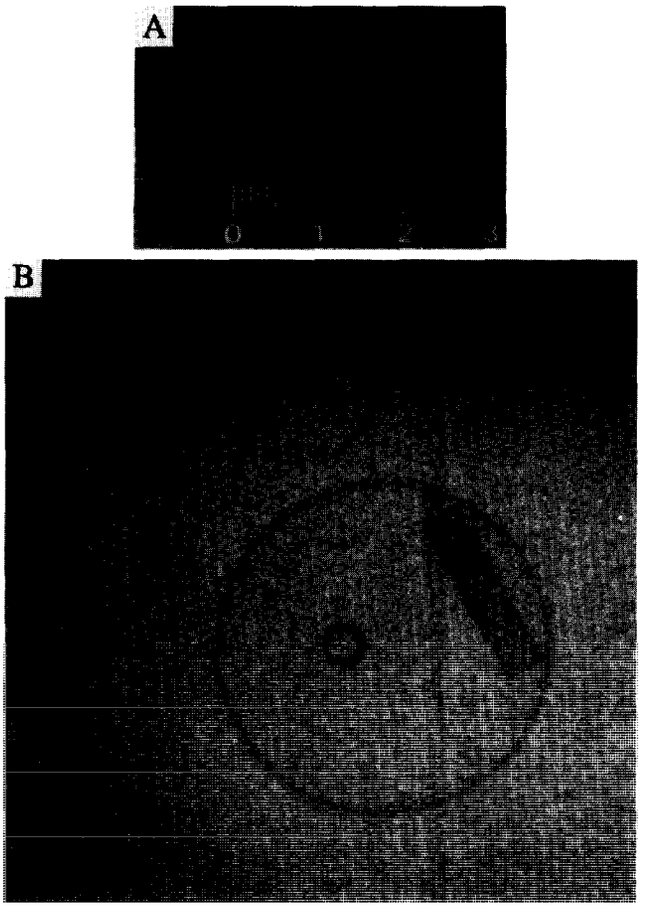

Figure 9 **A,** Stent prototype, made out of polymer B. Dimensions of the stent are: length 20 mm, outer ∅5 mm, inner ∅3.5 mm, and radial perforations ∅0.88 mm. **B,** Fluoroscopic image of two stent prototypes placed on a circular petri dish. One of the stents is in the horizontal position; the other in vertical position. Note that the perforations are clearly visible in the horizontal stent.

become the most common method for treatment of obstructive coronary atherosclerosis. Revascularization via PTCA is associated with two important limitations, *i.e.*, acute closure of the coronary artery (incidence ≈5%), and restenosis (incidence ≈35%). Stents are used to modify the rates of both acute occlusion and restenosis. The stents used in current practice are constructed out of metals, e.g. stainless steel or tantalum. It is generally believed that stent performance can be increased further through the use of less thrombogenic polymeric materials.

Figure 9A shows a stent prototype, made out of polymer B. The stent is a tubular object (outer ∅5 mm, inner ∅3.5 mm, length 20 mm), with radial perforations (∅0.88 mm). *Figure 9B* shows a fluoroscopic image of two of these stent prototypes placed on a circular petri dish. One of the stents is in the vertical position, and the other is in horizontal position. Note that the perforations are clearly visible in the horizontal stent.

The radiographic image of *Figure 9B* was recorded under realistic clinical conditions; we also verified that the stent is clearly visible if placed on top of a patient's chest.

The major advantages of stents as shown in *Figure 9* would be: (i) that the construction is much less thrombogenic than metals, currently used for the construction of stents; (ii) that it is possible to locate the stent continuously during the process of implantation; (iii) that deployment of the stent can be monitored directly. The major disadvantage is probably that the stents are permanent, as opposed to so-called biodegradable stents.

Finally, it may be important to note that it is possible, at least in principle, to change the composition of the polymer, or to add constituents, in order to abolish the phenomenon of retarded restenosis. Ideally, a thin, smooth re-endothelialized surface should be formed, and the resulting internal diameter should be sufficient to permit unimpended blood flow. While we realize that an ideal stent may not be realizable in practice, we feel that the approach via chemical synthesis of new radio-opaque polymeric materials, guided by a thorough understanding of the fundamental aspects of restenosis and re-endothelialization, holds considerable promise.

CONCLUSIONS

Polymers A–C are representatives of a new class of polymeric materials, which combine X-ray visibility and relatively low thrombogenicity. We feel that these materials hold considerable promise with respect to the construction of cardiovascular devices with improved performance. One particular application concerns endovascular stents: our radio-opaque polymers are likely to offer important advantages over the metallic materials, which are currently used for the construction of stents. Further work along these lines is currently in progress in our institute.

ACKNOWLEDGEMENT

The authors thank Mr L.J.M. van de Ven (Department of Instrumental Analysis, Eindhoven University of Technology) for recording and interpreting the solid-state NMR data.

REFERENCES

1 Ratner BD. New ideas in biomaterials science—a path to engineered biomaterials. *J Biomed Mater Res* 1993; **27:** 837–850.

2 Langer R, Peppas NA. Chemical and physical structure of polymers as carriers for controlled release of bioactive agents: A review. *J Macromol Sci Rev Macromol Chem* 1993; **23;** 61.

3 Peppas NA, Langer R. New challenges in biomaterials. *Science* 1994; **263:** 1715–1720.

4 Davies JP, O'Connor DO, Burke DW, Harris WH. Influence of antibiotic impregnation on the fatigue life of Simplex P and Palacos R acrylic bone cements, with and without centrifugation. *J Biomed Mater Res* 1989; **23:** 379–397.

5 Nimb L, Stürup J, Steen Jensen J. Improved cortical histology after cementation with a new MMA-DMA-IBMA bone cement: An animal study. *J Biomed Mater* 1993; **27:** 565–574.

6 Black J, Livingstone C. *Orthopaedic Biomaterials in Research and Practice.* New York: Churchill Livingstone; 1988: 133–161.

7 Mark HF, Bikales NM, Overberger CG, Menges G, eds. *Encyclopedia of Polymer Science and Engineering*; Vol. 14, 2nd edn., New York: John Wiley & Sons; 1988; 1–8.

8 Kruft MAB, Benzina A, Bär F, van der Veen FH, Bastiaansen CWM, Blezer R, Lindhout T, Koole LH. Studies on two new radio-opaque polymeric biomaterials. *J Biomed Mater Res* 1994; **28:** 1259–1266.

9 Benzina A, Kruft MAB, Bär F, van der Veen FH, Bastiaansen CWM, Heijnen V, Reutelingsperger C, Koole LH. Studies on a new radio-opaque polymeric biomaterial. *Biomaterials* 1994; **15:** 1122–1128.

10 Lindhout T, Blezer R, Maassen C, Heynen V, Reuteling sperger CPM. Platelet procoagulant surface as an essential parameter for the *in vitro* evaluation of the blood compatibility of polymers. *J Mater Sci, Mater Med* 1995; **6:** 367–372.

11 Sakariassen KS, Aarts PAMM, de Groot PG, Houdijk WPM, Sixma JJ. A perfusion chamber to investigate platelet interaction in flowing blood with human vessel wall cells, their extracellular matrix and purified components. *J Lab Clin Med* 1983; **102:** 522.

12 Jayakrishnan A, Chithambara Thanoo B. Synthesis and polymerization of some iodine-containing monomers for biomedical applications. *J Appl Polym Sci* 1992; **44:** 743–748.

13 Fox TG. Influence of diluent and copolymer compounds on the glass temperature of a polymer system. *Bull Am Phys Soc* 1956; **1:** 123.

14 Brandrup J, Imergut EH, eds. *Polymer Handbook*; Vol. 6, 3rd edn., New York: John Wiley & Sons, 1989: 218–219.

15 Mark HF, Bikales NM, Overberger CG, Menges G, eds. *Encyclopedia of Polymer Science and Engineering*; Vol. 5, 2nd edn., New York: John Wiley & Sons, 1988: 299–329.

16 Mark HF, Bikales NM, Overberger CG, Menges G, eds. *Encyclopedia of Polymer Science and Engineering*; Vol. 1, 2nd edn., New York: John Wiley & Sons, 1988: 260.

17 Hemker HC, Willems GM, Béguin SA. A computer assisted method to obtain the prothrombin activation velocity in whole plasma independent of thrombin decay processes. *Thromb Haemost* 1986; **56:** 9–17.

18 Sigwart UC, Frank GI, eds. *Coronary Stents*, Berlin: Springer-Verlag; 1992: 5–19.